



Groundwater pollution risk assessment using a calculated contamination index and geostatistical analysis: Jerba Island case study (southeast of Tunisia)

Faiza Souid¹ · Mohamed Hamdi² · Mohamed Moussa¹

Received: 19 March 2022 / Accepted: 21 September 2022 / Published online: 30 September 2022
© Saudi Society for Geosciences 2022

Abstract

In this study, the groundwater contamination degree in the unconfined coastal aquifer Jerba under arid climate (Southeastern Tunisia) was investigated, and a new index, groundwater contamination index (GCI), was calculated and combined with the geostatistical analysis and the self-organizing maps (SOM). The groundwater samples used in this research were collected from 79 groundwater wells during the dry season (August–October 2014). Hydrochemical parameters (Cl^- , Br^- , Na^+ , Ca^{2+} , Mg^{2+} , K^+ , SO_4^{2-} , NO_3^- , NO_2^- , HCO_3^- , Li^+ , and F^-) and indicator bacteria of fecal contamination (total coliforms, thermotolerant coliforms, and *Escherichia coli*) were analyzed. The GCI was calculated based on selected indicator parameters notably NO_3^- and Li^+ , measured seawater fraction based on chloride balance, and fecal bacteria tracers. Geostatistical modeling was used for assessing and mapping groundwater contamination degrees. Ordinary Kriging was adopted for spatial interpolation to study the spatial pattern of the groundwater hydrochemical variables over the island using GIS software ArcGIS 10.1. The SOM method was adopted to analyze the relationship between ions and identify processes controlling groundwater salinization. According to the GCI, most of the unconfined aquifer (76%) comes under the significant pollution zone (high to moderate pollution), and the other areas (24%) are defined as areas with low degrees of pollution. The self-organizing maps (SOM) indicated that Cl^- , Br^- , and Na^+ emanate mainly from seawater intrusion and Mg^{2+} , Ca^{2+} , and Li^+ are mostly derived from rock-water interactions. Results show that the new index is robust and gives the best classification of groundwater quality.

Keywords Groundwater contamination degree · Kriging · Geostatistic · Coastal aquifer · Jerba Island

Introduction

In regions under arid and semiarid climate conditions worldwide, groundwater is a major source of water supply (Patel et al. 2020; Carol et al. 2021; Silva et al. 2021). The identification of key processes governing groundwater mineralization is based on geochemical tracers such as nitrogenous elements (Souid et al. 2017; Solgi and Jalili 2021; Zhang et al. 2021); conservative elements

(Cartwright et al. 2006; Alcalá and Custodio 2008; McArthur et al. 2012; Souid et al. 2018); isotopic tracers: stable isotopes of water (Souid et al. 2020; Mahlangu et al. 2020); nitrogen isotopes (Kou et al. 2021; He et al. 2022a); isotopes of metal pollutants; radioactive tracers: radon, uranium (Milena-Pérez et al. 2020; Mathuthua et al. 2020), tritium (Nigro et al. 2017; Mahlangu et al. 2020), and carbon (Innocent et al. 2021); and biomarkers of fecal contamination: total and thermotolerant coliforms, *E. coli*, and salmonella (Han Tran et al. 2015; Souid et al. 2017).

Obtaining the highest possible compatibility between “ideal” and “possible” scenarios is one of the most difficult aspects of any environmental management system (Barilari et al. 2020). Groundwater quality and risk assessments include a variety of quantitative methods, such as mathematical groundwater flow modeling and the transportation and the evaluation of pollution plume. These strategies will be of limited utility to groundwater managers who need to achieve proactive and timely groundwater protection across large aquifers (Somaratne et al. 2013). There are other qualitative procedures for assigning a label

Responsible Editor: Broder J. Merkel

✉ Faiza Souid
faizasouid@gmail.com

¹ Laboratory of Eremology and Combating Desertification (LR16IRA01), Institut des Régions Arides—IRA, University of Gabès, 4119 Medenine, Tunisia

² CARTEL - Centre d'applications Et de Recherche en Télédétection, Faculté Des Lettres Et Sciences, Humaines de L'Université de Sherbrooke, Québec, Canada

based on land use (Zaporozec 2004) as well as intermediate methodologies known as index methods, which include aquifer vulnerability assessment tools (e.g., DRASTIC, GALDIT, and GOD coupled to geophysical information system), and water quality index (Nsabimana et al. 2021). Methodological approaches that integrate numerous groundwater quality variables in a specific index to assess pollution degrees have found widespread uses in environmental science and engineering (Wagh et al. 2018; Herojeet et al. 2020).

In the Mediterranean regions, salinization is the major concern for coastal aquifers because of climate change and overexploitation (Nisi et al. 2022). In addition to their relative scarcity, Tunisia's groundwater resources, especially those of the shallow aquifers, are often of poor quality. Thus, about 12% of groundwater resources are characterized by salinity lower than 3 g/l. The overexploitation results in the degradation of the groundwater quality with an increase in the salinization and contamination risks. Overexploitation also leads to the lowering of the piezometric levels. In addition, the various forms of pollution that affect the unconfined aquifers make the groundwater sometimes unfit for domestic use (Elloumi 2016). Moreover, Tunisian groundwater resources have been exploited excessively in recent years, causing the depletion of reserves of many aquifers. The volume extracted from aquifers is estimated at 480 Mm³/year, or 24% of total withdrawals of groundwater, which is hardly sustainable. According to the 2004 national inventory, there were 750 sources of contamination with urban, industrial, and agricultural origins that are likely to seriously affect groundwater supplies. The inventory notes more than 40 urban water treatment plants that do not comply with the Tunisian standard of discharge into the aquatic environment. The food industry is the primary source of pollution, followed by the sectors of textile and clothing, rubber, and plastic (Besbes et al. 2014).

Jerba unconfined aquifer is a coastal aquifer under an arid climate. It is influenced by several factors: climate conditions, anthropic activities, and seawater intrusion. This aquifer was decreed as a safeguard area of groundwater resources (Decree N°. 85–1108 of 29 August 1985-Tunisia). The previous hydrogeological studies carried out on the shallow aquifer of Jerba Island focus on the geochemical processes of groundwater salinization based on geochemical and statistical modeling and the assessment of groundwater piezometry (Kharroubi et al. 2012; Telahigue et al. 2018; Souid et al. 2017, Souid et al. 2020). Such studies demonstrate the deterioration of the groundwater geochemical quality. The lack of a sustainable groundwater exploitation management strategy has worsened the situation on the island. The novel contribution of this work is to propose an empirical index based on a contamination tracer to facilitate the understanding of the aquifer contamination processes.

The aim of the present research is to study the groundwater contamination degree of an arid coastal aquifer known by the scarcity of water resources and an aquifer system subjected to

many natural and human pressures. The specific objectives were to identify the causes of groundwater pollution for a better monitoring and recognize the threats to groundwater supply, based on a contamination index (combining chemical and bacteriological tracers of contamination) and geostatistical approaches. Jerba Island's unconfined aquifer in the southeast of Tunisia is used as a study case.

Methodology and data processing

Location of the study area

The area of research is in Tunisia's southeast between latitude 33°38' and 33°56'N and longitude 10°43' and 11°04'E. It occupies an area of about 514 Km² (Fig. 1). The annual average rainfall is 250 mm, and the annual average evaporation is 1082 mm (Souid et al. 2020). Surface waters mainly consist of rainwater stocked in special tanks and used for drinking and domestic purposes. The island's topography is flat, with an average altitude of 50 m. The island is covered by quaternary sediments composed, as shown in the hydrogeological cross-section (Fig. 1), by a thick-bedded Mio-Plio-Quaternary sand and clay overlying bedrock downwards and upwards by the gypseous crusts attributed to Villafranchian. The shoreline of the island is draped by the marine facies of Holocene and Pleistocene. The Mio-Pliocene marl and clay act like an aquitard, while the Mio-Pliocene sand represents the basal aquifer (Teissier 1967; Jedoui 2000; Bouaziz et al. 2003; Yahyaoui 2012).

The underground of the island encloses a phreatic aquifer and a deep confined aquifer (Fig. 1), within the quaternary sediments separated vertically by a thick clay layer that represents the aquitard stratum. The unconfined aquifer, which is mainly composed of lenticular sandy levels of Quaternary upper Pleistocene and Quaternary Holocene, is the most used aquifer level by the locals for both domestic and agricultural purposes (Kharroubi et al. 2012; Yahyaoui 2012; Souid et al. 2017). The unconfined aquifer in the island is mostly recharged by the vertical rainwater infiltration and surface water (irrigation water and wastewater) infiltration. The aquifer depth ranges between 3 and 50 m with a mean depth of 30 m. The unsaturated zone is mainly made up of Mio-Plio-Quaternary sandy loam, silt loam, and sand layers. Overexploitation has led to the continuous decline in the aquifer's piezometric level (Souid et al. 2017, 2020).

Physicochemical and bacteriological analyses

A total of 79 groundwater points were sampled, after purging for 5 min to verify that the groundwater samples were reflective of the in situ conditions, during the summer season

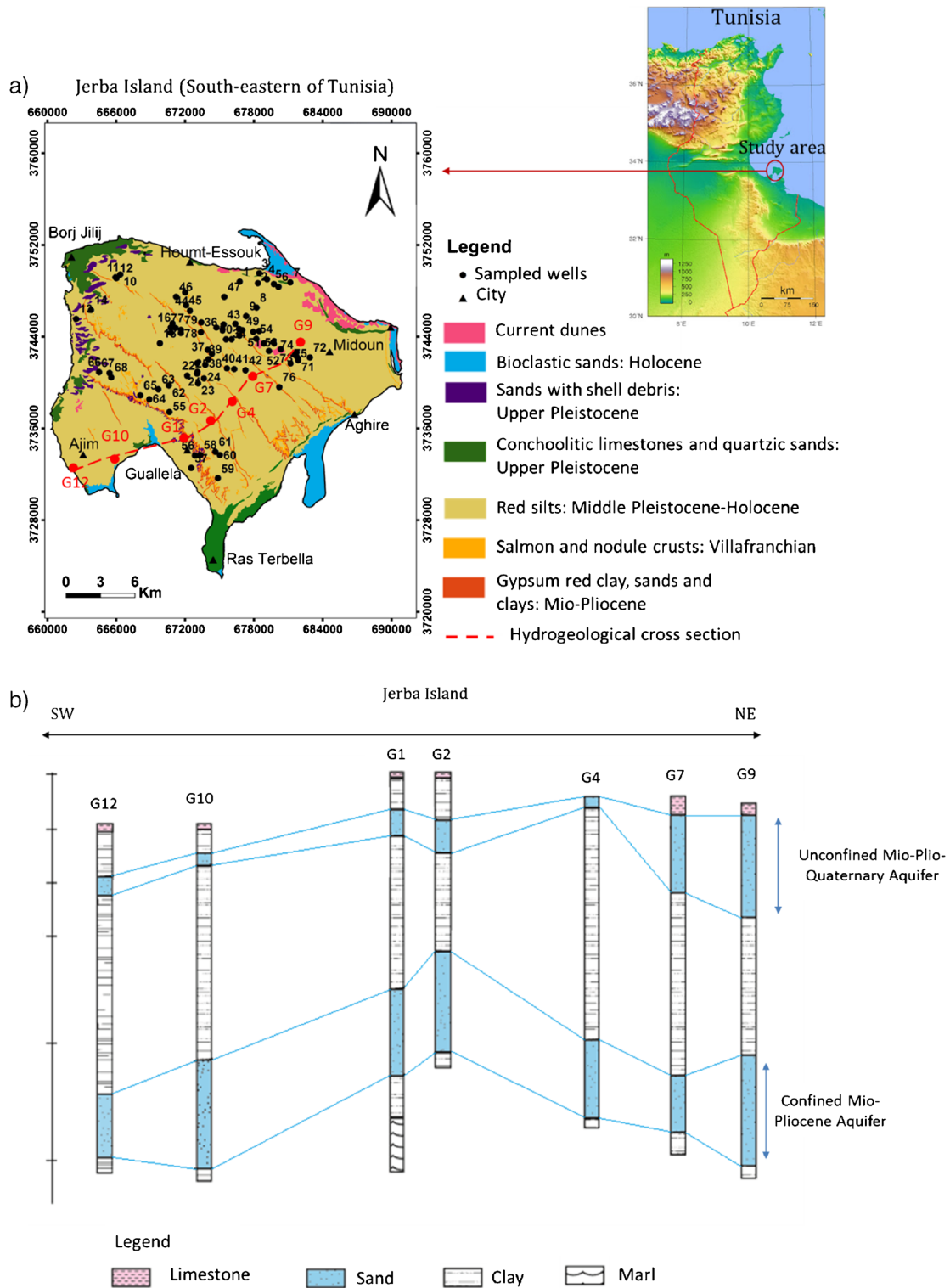


Fig. 1 a Geological map of the of the Jerba Island; b hydrogeological cross-section

(August–October 2014). Samples for the enumeration of fecal contamination tracers were stored in a sterile glass container (200 ml). For physicochemical analyses, groundwater samples were kept in polyethylene bottles (500 ml). During the

groundwater sampling, EC, salinity, and pH were measured on the field using a Consort 933 multi-parameter. Cations (Na^+ , K^+ , Ca^{2+} , Mg^{2+} , Li^+) and anions (Cl^- , Br^- , NO_3^- , NO_2^- , SO_4^{2-} , HCO_3^- , F^-) were analyzed using chromatography (ionic

liquid chromatograph Metrohm 850). Prior to analysis, the filtration of water samples through cellulose membrane (pore size: 0.45 μm) was carried out. Samples were kept cool and transported to the laboratory of the Higher Institute of Water Sciences and Techniques, University of Gabes, Tunisia. To assess the quality control measures of chemical analyses, ionic balance errors (within 10%) were calculated.

The membrane filtration standard (ISO 9308–1 2000) was adopted to enumerate total (TC) and thermotolerant coliforms (Thc). The seeding of these bacteria was carried out on the bacterial culture medium Tergitol TTC Agar during 42 h of incubation. The incubation temperature is 37 °C for TC and 40 °C for Thc. The enumeration results were expressed by CFU 100 ml^{-1} unit. Total coliform colonies were transplanted on a tryptophan reagent to identify *Escherichia coli* bacteria. The identification of *E. coli* in aqueous media was confirmed after an incubation time of 24 h at a temperature of 44 °C. *E. coli* bacteria cause indole production, which can be determined by adding Kovac's reagent. Bacteriological analyses were performed at Tunisia's Public Health Ministry's Regional Hygiene Laboratory in Jerba.

Geostatistical analysis

A histogram and standard QQPlot tools were used to verify the normality of the distribution pattern in the geochemical dataset. Normal QQPlot is a graphical normality assessment method to indicate univariate normality (Johnston et al. 2001), investigate the distribution of data, and look for outliers. For that, The Shapiro–Wilk and Kolmogorov–Smirnov tests were performed to assess the normality of the dataset. The normality tests are used in addition to the graphical normality evaluation (Elliott and Woodward 2007). These statistical tests compare the scores in the samples to a Gaussian distribution of scores, which presents a normally distributed set, with the same mean and standard deviation. If the “*P*” value of the tests is more than 5%, the null hypothesis is accepted and “sample distribution is Gaussian.” If the test is significant (“*P*” value of the tests is less than 5%), the distribution is non-Gaussian (Ghasemi and Saleh Zahediasl 2012). The Kolmogorov–Smirnov test is an empirical distribution function that compares the test distribution's theoretical cumulative distribution function to the data empirical distribution function (Oztuna et al. 2006). The Shapiro–Wilk test is more efficient than the Kolmogorov–Smirnov test since it is based on the correlation between the data and the matching normal scores (Peat and Barton 2005).

Semivariograms are used to quantify the spatial autocorrelation (dependence) between sampled points. The semivariogram is based on the simple geographic dogma: samples that are close to each other are more similar on the geochemical behavior than the more distant samples. This principle is called autocorrelation (statistical and spatial relationships between samples). Experimental semivariogram and experimental covariance were calculated based on Eqs. (1) and 2, respectively:

$$\gamma(h) = \frac{1}{2n(h)} \sum_{i=1}^{n(h)} (Z(x_i) - Z(x_{i+h}))^2 \quad (1)$$

where $n(h)$ is the pair number of the studied data within a specified range of equidistance and direction. When the variables $Z(x_i)$ and $Z(x_{i+h})$ are auto-correlated, the estimated value $Z^*(x_0)$ (the result of Eq. 4) is small, and thus, the pair of points is spatially uncorrelated. Based on the analysis of the empirical variogram (experimental variogram), a suitable mathematical variogram model (e.g., Gaussian, spherical, exponential) is then adjusted, usually by weighted least squares, and variogram parameters (range, nugget, and sill) are then used in the Kriging approach (Zare-Mehrjardi et al. 2010).

If the random variable pair x_i and x_{i+h} can take on the values $Z(x_i)$ and $Z(x_{i+h})$ for $i = 1, \dots, n$ with equal probabilities, $p_i = \frac{1}{n}$, then the covariance can be expressed in terms of means $Z(x_i)$ and $Z(x_{i+h})$ as:

$$C(h) = \frac{1}{n(h)} \sum_{i=1}^{n(h)} [(Z(x) - Z(x_i))(Z(x+h) - Z(x_i+h))] \quad (2)$$

For a model that provides accurate unsampled point estimations, the standardized mean (SM) error should be close to 0, the root-mean-square error (RMSE) and average standard error (ASE) should be as small as possible (comparing obtained values for each tested model), and the RMSS should be close to 1 (Johnston et al. 2001). The smallest RMSE indicates the most accurate predictions. The RMSE was derived according to Eq. (3) (Zare-Mehrjardi et al. 2010):

$$RMSE = \sqrt{\frac{1}{N} \sum_{i=1}^N (Z(x_i) - Z^*(x_i))^2} \quad (3)$$

$Z(x_i)$ is the measured observation at the position x_i , $Z^*(x_i)$ is the estimated observation at the position x_i , and N is the sample number.

Ordinary Kriging was adopted to assess the spatial pattern of the studied groundwater hydrochemical variables over the island. The GIS software ArcGIS 10.1 was used for spatial interpolation in this work. Kriging may be considered the most efficient method for prediction (interpolation) at unsampled areas. This geostatistical approach permits the study of spatial autocorrelation between the investigated variables. One of the most significant advantages of the Kriging method is that it provides for the estimation of the error interpolation values of the regionalized variable when there are unsampled sites, providing a measure of the estimation accuracy and reliability of the variable's spatial distribution (Burgess and Webster 1980). The general equation of the Kriging estimator is:

$$Z^*(x_0) = \sum_{i=1}^n \lambda_i Z(x_i) \quad (4)$$

For each groundwater sample, the hydrochemical data were inserted into a digital database and GIS, using ArcGIS v10.1.

For spatial distribution maps, a histogram and a normal QQPlot analysis were performed. It was observed that the data are approximately normally distributed. Table 1 shows the results of the normality tests. It is clear that all variables, for both tests, have a *P* value less than 0.05, which indicates a non-Gaussian distribution of data, except for the GCI parameter. Log transformation was applied for the parameters that have a non-normal distribution to obtain a normal distribution.

Prediction model performances were assessed by cross-validation. Table 2 presents the selected model characteristics for the studied groundwater quality parameters. The mathematical models of semivariograms (Gaussian, exponential, circular, or spherical models) were tested for salinity, GCI, and seawater fraction. The models provide information about the spatial distribution including the Kriging interpolation input parameters (Boudibi et al. 2021a; Hatvani et al. 2021). The adequate model for interpolation is selected referring to the calculated error values (Table 2). The SM error is close to 0 for all studied parameters, the RMSE and ASE are low comparing to obtained values for each tested model, and RMSS is closer to the RMSE. The cross-validation results clearly indicated that circular and spherical semivariogram models are the fitted models to the spatial interpolation of the dataset.

Calculated groundwater contamination index (GCI)

A contamination index is a useful tool that can be applied to assess groundwater pollution. Various indices have been used by researchers to assess groundwater contamination (Adimalla et al. 2020; Herojeet et al. 2020; Serra et al. 2021). The groundwater contamination index provides a

single value which summarizes the big dataset of quantity parameters and represents data in a simple way. GCI is an effective approach for assessing and mapping the degree of groundwater pollution (Kumar 2014). In this work, a new index is formulated and proposed to evaluate the intensity of groundwater pollution in the Jerba shallow aquifer. The different steps involved in the research process are shown by the flow chart (Fig. 2).

The calculated contamination index was derived from the combination of chemical and bacteriological parameters. The combination of chemical and bacteriological tracers helps to highlight pollution from natural and anthropogenic sources (Fig. 3). The selection of the parameters integrated in the calculation of the index was based on the indicators most involved in the geochemical signature of the groundwater. This means that a specific tracer has been chosen for each contamination process to assess the contamination degree of the aquifer. In this study, lithium and nitrate concentrations, seawater fraction, and fecal indicator bacteria (TC and ThC coliforms and *Escherichia coli*) were used as tracer parameters to measure the pollution degree. Weights are assigned to each parameter chosen for the proposed index depending on a number of factors, including health risk and importance in assessing groundwater quality (Herojeet et al. 2020). Pollution degrees ranged into six classes according to the concentration of each parameter (Table 3). For each parameter, the values were grouped by importance to three clusters:

- Low pollution degree cluster: this class includes the low values. For this class, the pollution degree is considered low.
- Medium pollution degree cluster: this group is composed of medium values. The pollution level of this cluster is medium.
- High pollution degree cluster: high values of each parameter are included in this cluster.

Table 1 Normality test results

	Tests of normality							
	Kolmogorov–Smirnov with Lilliefors Significance Correction				Shapiro–Wilk			
	Statistic	df	<i>P</i> value	Interpretation	Statistic	df	<i>P</i> value	Interpretation
Salinity	0.118	79	0.008	NGD	0.958	79	0.011	NGD
Seawater fraction	0.118	79	0.009	NGD	0.929	79	0.000	NGD
GCI	0.115	79	0.061	GD	0.967	79	0.126	GD

GD, Gaussian distribution (*P* > 0.05); NGD, non-Gaussian distribution (*P* < 0.05)

Table 2 Experimental semivariograms and fitted models of GCI, salinity, and seawater fraction

Parameter	Semivariogram	RMSE	ASE	SM	RMSS	Range	Nugget	Partial sill
GCI	Circular	3.07	2.93	0.01	1.04	8.6 × 10 ³	0.001	1.23
Salinity	Spherical	1.48	1.32	0.01	1.1	6.63 × 10 ³	0.5	4.36
Seawater fraction	Circular	4.68	3.98	0.01	1.16	9.09 × 10 ³	8.44	37.27

Fig. 2 Flow chart showing the different steps involved in the research process

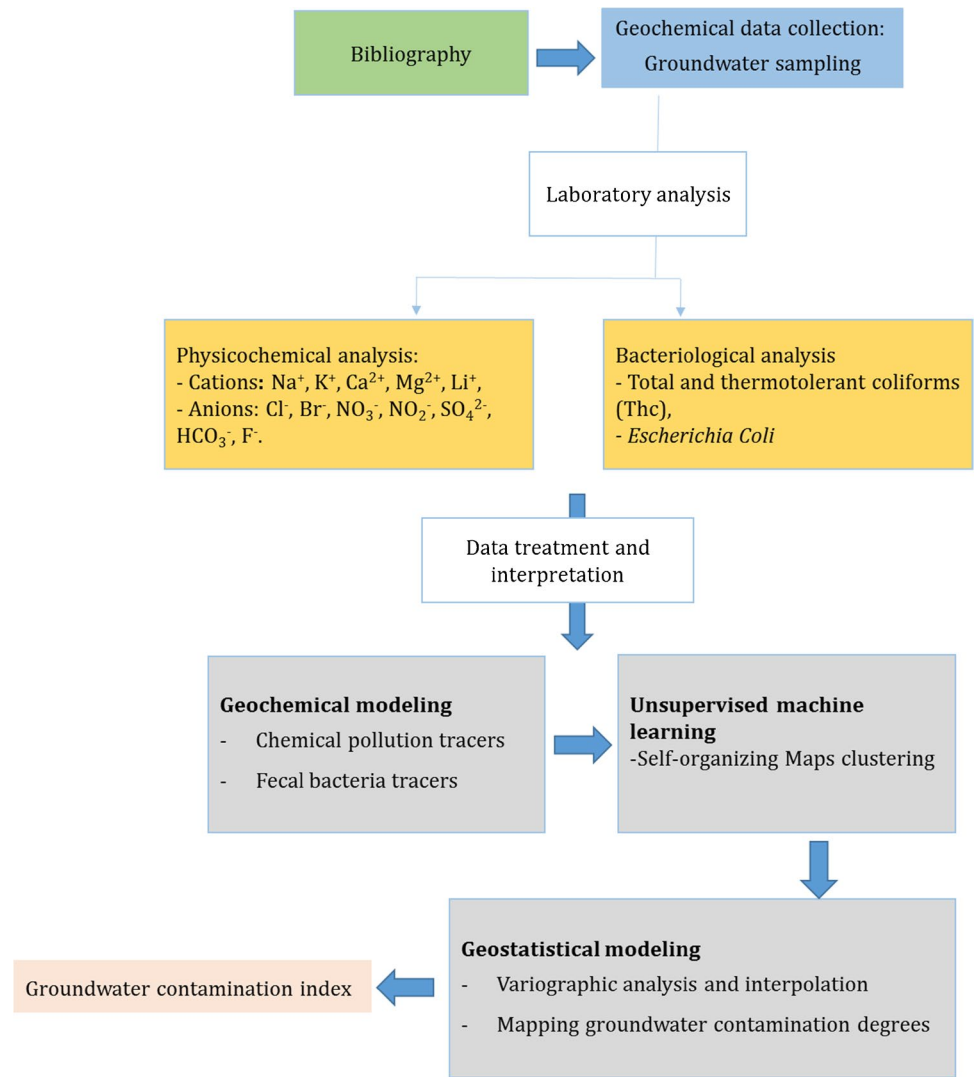
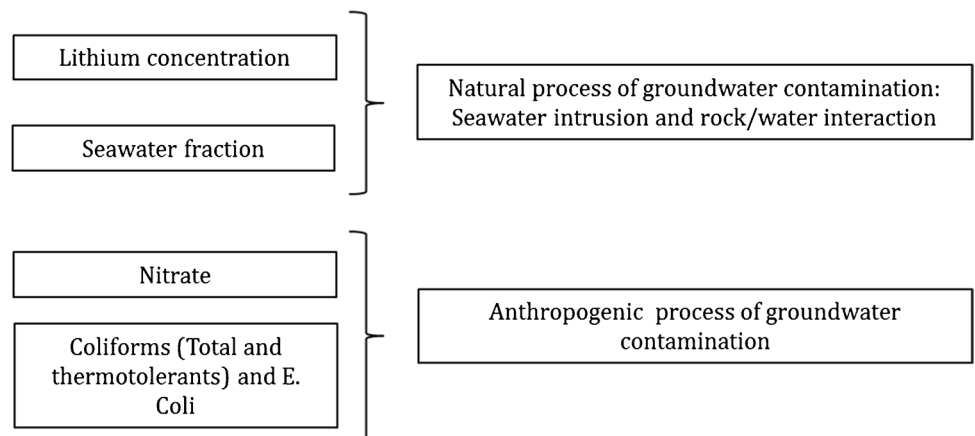


Fig. 3 Parameters used to calculate groundwater contamination index (GCI)



To calculate the GCI, three steps were required. In the first step, each parameter (lithium, nitrate, seawater fraction, total and thermotolerant coliforms and *E. Coli*) was assigned a relative weight (class) ranging from 1 to 6 based on its

contents. The lowest values received the lowest weight (1), while the highest values received the highest weight (6). In the following step, the weight for each parameter was calculated to determine its relative contribution to the process of

groundwater contamination. At the end of the process, the contamination index is calculated by adding the pollution degree classes assigned to each parameter. The groundwater contamination index was calculated as the weighted sum of all contamination class degrees (Eq. 5):

$$GCI = \sum_{i=1}^n C_i \tag{5}$$

where C_i is the single contamination class degree of each tracer parameter.

Results and discussion

Hydrogeochemistry

Basic statistics of the studied parameters (Table 4) show that the standard deviation values are low for all variables (parameters) compared to the means. The dataset distribution assessment based on skewness and kurtosis demonstrates that the fluoride distribution is right-skewed (negative skewness). The rest of the hydrogeochemical parameters are right-skewed (positive skewness). The statistical distribution form is platykurtic (kurtosis < 0) for pH, EC, salinity, HCO_3^- , Cl^- , Br^- , SO_4^{2-} , Na^+ , and Ca^{2+} and leptokurtic (kurtosis > 0) for F^- , NO_3^- , NO_2^- , K^+ , Mg^{2+} , and Li^+ .

Salinity rates range from 8.8 in the shoreline to 0.5 g/l in the inner regions of the island. The hydrochemical fingerprint of Mio-Pliocene–Quaternary Jerba aquifer is characterized by Na-Cl groundwater facies type (Fig. 4). For a coastal aquifer in an arid climate, the high levels of Cl^- (the average concentration is about 1738.56 mg/l) and Na^+ ions (with a mean concentration of 1107.96 mg/l) were due to the seawater impact on groundwater hydrogeochemical signature. Referring to the average concentrations, chloride is considered as the most abundant ionic species in the chemical composition of analyzed groundwater samples. Chemical contamination tracers like NO_3^- , NO_2^- , F^- , and K^+ are plentiful in the aquifer. The highest concentration was measured

for nitrate with average values of 75.97 mg/l. Li^+ concentrations of groundwater points ranged between 1 and 14 mg/l.

The correlation between salinity and chemical elements was assessed using Pearson correlation (for normal distribution) to establish the relationship between ions and aquifer abnormal salinization. A P value of < 0.01 is considered to be significant. The correlation matrix (Table 5) measures the strength of the correlation among groundwater mineralization, Ca^{2+} , Mg^{2+} , K^+ , Li^+ , Cl^- , and Br^- . These findings demonstrate the importance of these ions in the groundwater salinization processes of Jerba unconfined aquifer. The feature maps generated by the application of unsupervised machine learning technique, i.e., SOM, confirm the obtained results (Fig. 5). The maps (grid) of the studied variables (salinity, Ca^{2+} , Mg^{2+} , K^+ , Li^+ , Cl^- , and Br^-) of the dataset display the trends of statistical correlation between ions and mineralization. The similar neuron patterns in the grids (the coloring of the map) indicate the positive correlation between studied parameters. The Kohonen map clustering method proves the significant correlations among salinity, halogens (Cl^- and Br^-), alkaline earth metals (Ca^{2+} and Mg^{2+}), and alkali metals (Na^+ , K^+ and Li^+).

The selected groundwater contamination index parameters

Lithium

The maximum content of Li^+ ion amounts to 15.69 mg/l. The abundance of this alkaline metal is assigned to groundwater-aquifer rock interactions related to cation-exchange reactions caused by seawater mixing. With reference to the hydrogeological study by Souid et al. (2018) on this coastal aquifer, lithium can be used as a salinization, resulting from the seawater invasion process, chemical proxy. As a result of the ion exchange mechanism, the content of this alkaline metal significantly increases corresponding to the seawater fraction. The use of this chemical element as a salinization ion tracer justifies its selection for the calculation of the index.

Table 3 Classes of the parameters used to calculate GCI

Pollution degree	Low		Medium		High	
Class	C_{Li}	C_{NO_3}	C_{sf}	C_{TC}	C_{thC}	C_{Ec}
	1	2	3	4	5	6
Lithium concentration (mg/l)	> 2	2–4	4–6	6–8	8–10	> 10
Nitrate concentration (mg/l)	> 10	10–20	20–30	30–40	40–50	> 50
Seawater fraction	> 0	0–5	5–10	10–15	15–20	> 20
Total coliforms (UFC)	< 100	100–1000	1000–10,000	10,000–100,000	> 100,000	–
Thermotolerant coliforms (UFC)	Absent	< 10	10–100	100–1000	1000–10,000	> 10,000
<i>E. coli</i>	Absent	Present	Present	Present	Present	Present

Table 4 Statistical characteristics of the hydrochemical parameters

Parameters	Min	Max	Mean	Variance	S.D	Kurtosis	Skewness
pH	6.90	8.19	7.52	0.07	0.27	-0.13	0.16
Salinity (mg/l)	514	8882	3799.43	4,327,173.71	2080.19	-0.63	0.49
CE (mS/cm)	1.04	15.26	6.86	12.53	3.54	-0.71	0.41
TDS (mg/l)	665	9760	4387.14	5,125,075.63	2263.66	-0.71	0.41
HCO ₃ ⁻ (mg/l)	136.89	664.42	401.84	16,561.06	128.69	-0.69	0.37
F ⁻ (mg/l)	3.95	6.83	6.01	0.27	0.52	4.70	-1.67
Cl ⁻ (mg/l)	136.57	4319.83	1738.56	1,161,230.60	1077.60	-0.54	0.58
Br ⁻ (mg/l)	8.75	12.32	10.35	0.68	0.83	-0.80	0.19
NO ₃ ⁻ (mg/l)	39.32	196.89	75.97	1487.00	38.56	0.65	1.16
NO ₂ ⁻ (mg/l)	14.02	80.85	23.99	129.05	11.36	7.08	2.13
SO ₄ ²⁻ (mg/l)	56.31	1178.56	569.44	63,284.62	251.56	-0.02	0.24
Na ⁺ (mg/l)	223.42	2601.97	1107.96	332,198.75	576.37	-0.64	0.47
K ⁺ (mg/l)	12.05	154.65	56.23	862.54	29.37	0.41	0.76
Ca ²⁺ (mg/l)	68.98	754.56	301.48	23,567.01	153.52	-0.20	0.61
Mg ²⁺ (mg/l)	20.63	437.97	149.58	7378.86	85.90	0.41	0.75
Li ⁺ (mg/l)	1.12	15.70	5.68	9.03	3.00	0.37	0.74

Min, minimum; Max, maximum; S.D., standard deviation

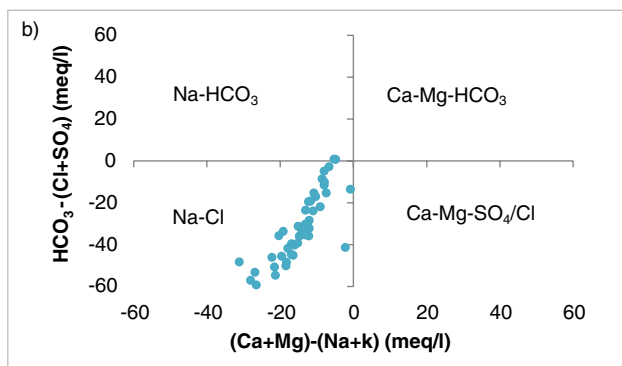


Fig. 4 Groundwater facies based on $(Ca+Mg)-(Na+K)$ vs. $HCO_3-(Cl+SO_4)$

Seawater fraction (f_{sea})

In this study, the seawater fraction is calculated based on Cl^- content (Eq. 6). Considered as a conservative tracer, chloride is unaffected by water/rock reactions.

$$f_{sea} = \frac{C_{Cl,sample} - C_{Cl,fresh}}{C_{Cl,sea} - C_{Cl,fresh}} \quad (6)$$

where $C_{Cl,sample}$ is the measured chloride content of the sample, $C_{Cl,sea}$ is the chloride content of the Mediterranean sea sample, and $C_{Cl,fresh}$ represents the chloride content of the freshwater (the lowest analyzed salinity in groundwater samples).

Calculated seawater percentage varies between a maximum value of 18.73% and a minimum value of -0.83%

(Fig. 6). The estimated seawater fraction spatial distribution map was used to define the spatial expansion of seawater intrusion in the island (Fig. 7). The low seawater percentages are within the central and the eastern parts of the study area.

The groundwater salinity increase is due to intensive exploitation caused by overpumping, which leads to seawater intrusion into coastal aquifers, promoting vertical exchanges between the shallow aquifer and deep confined aquifer characterized by brackish groundwater. Based on GIS interpolation approaches, we estimated the geographical extent of groundwater salinization. Figure 7 shows that the spatial distribution of groundwater salinity is mapped to the piezometric level. Areas characterized by high piezometric levels, considered as recharging areas, have low salinity values. On the other hand, areas of low piezometric levels show high salinity values. The map clearly shows that around the shoreline, in which the groundwater level is as low as 0 m below ground level (mbgl), the trend indicates that depletion has occurred at a very fast rate.

Nitrate

Nitrate is naturally present in water, coming from the natural cycle of organic nitrogen degradation. The high levels of nitrate in groundwater are due to agricultural activities (irrigation and organic fertilizer like manure), livestock, or industrial and domestic sewage (Li et al. 2019; He et al. 2022a, 2022b). In fact, 95% of the nitrogen flow is in the form of nitrates, the organic and ammonia forms remaining insignificant in agricultural inputs (Koné et al. 2009;

Table 5 Correlation matrix

	Salinity	HCO ₃ ⁻	F ⁻	Cl ⁻	Br ⁻	NO ₃ ⁻	NO ₂ ⁻	SO ₄ ²⁻	Li ⁺	Na ⁺	K ⁺	Ca ²⁺	Mg ²⁺
Salinity	1.00												
HCO ₃ ⁻	0.29	1.00											
F ⁻	0.11	0.14	1.00										
Cl ⁻	0.99	0.26	0.12	1.00									
Br ⁻	0.79	0.39	0.14	0.79	1.00								
NO ₃ ⁻	0.46	0.14	-0.12	0.47	0.36	1.00							
NO ₂ ⁻	0.44	0.28	-0.06	0.43	0.40	0.91	1.00						
SO ₄ ²⁻	0.64	0.01	-0.04	0.54	0.40	0.15	0.21	1.00					
Li ⁺	0.98	0.38	0.13	0.96	0.79	0.39	0.40	0.60	1.00				
Na ⁺	0.99	0.37	0.13	0.98	0.80	0.46	0.45	0.59	0.97	1.00			
K ⁺	0.98	0.38	0.13	0.96	0.79	0.39	0.40	0.60	1.00	0.97	1.00		
Ca ²⁺	0.98	0.36	0.13	0.96	0.79	0.39	0.40	0.64	0.99	0.98	0.99	1.00	

Fig. 5 SOM maps for Cl⁻, Br⁻, Na⁺, Ca²⁺, Mg²⁺, and Li⁺

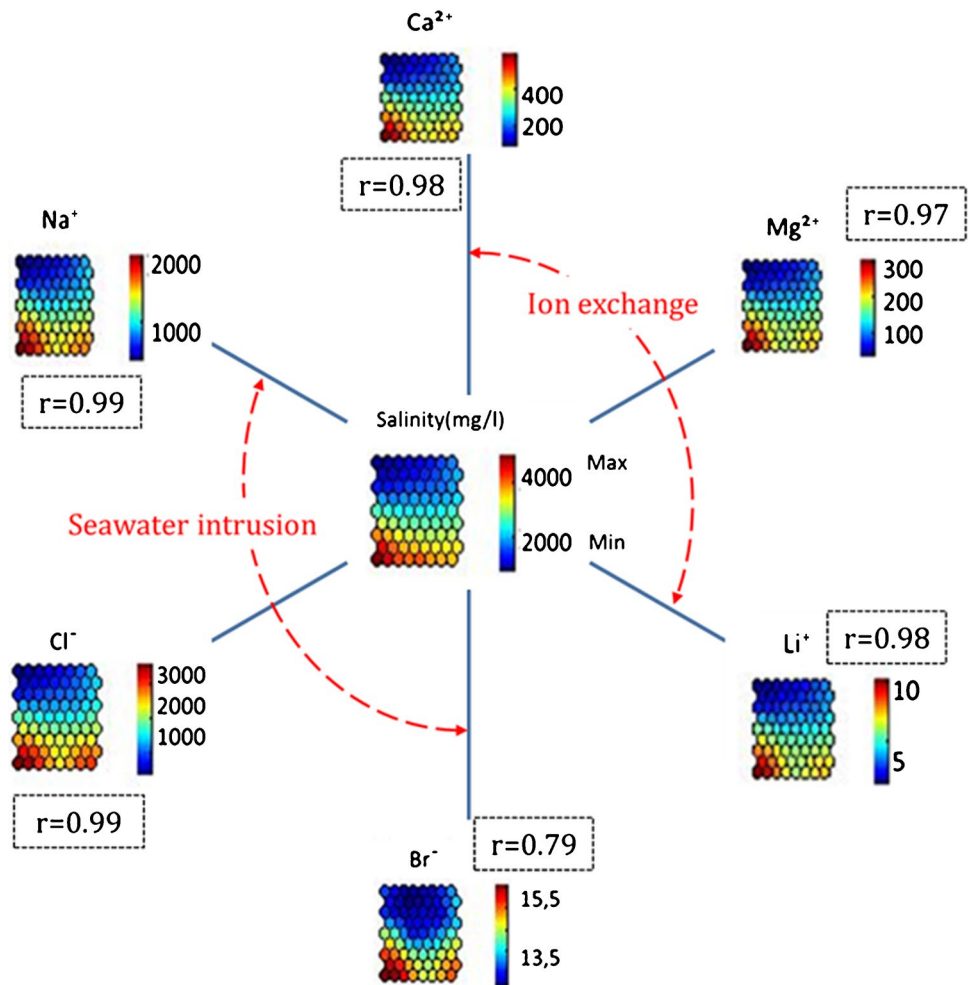
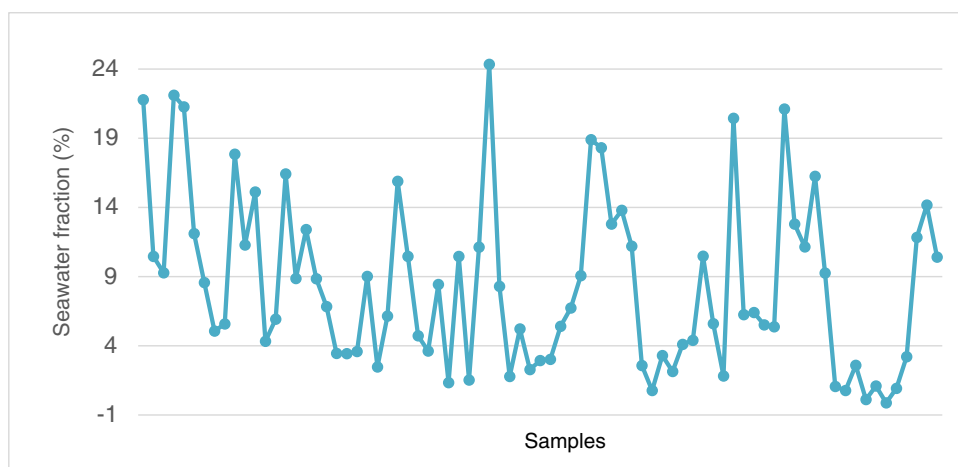


Fig. 6 Measured seawater fraction



Ma et al. 2009; Boudibi et al. 2021a). The Jerba shallow aquifer shows high levels of NO_3^- . The measured concentration of nitrate in sampled wells ranges from 39.32 to 196.89 mg/l. By comparing the nitrate levels with the standards set by the World Health Organization (WHO), which sets a threshold of 50 mg/l for NO_3^- , we note that 60.75% of the groundwater samples are beyond the standards and therefore unfit for human consumption. Referring to Fig. 8, NO_3^- concentration showed clear spatial variability. The absence of a sewer system in rural and suburban areas of the island contributes to the increase of nitrate concentration. In Jerba Island, rural domestic sewage is primarily composed of toilet effluent and greywater (water used in washing, bathing, and kitchen).

Coliforms (total and thermotolerant) and *E. coli*

Bacteriological analysis revealed that 94.9% of groundwater samples had TC densities greater than 10 CFU/100 ml. Except for three wells that were deeper than 50 m, all samples were tested positive for Tbc and *E. coli*. The wastewater discharge in rural regions of the island generates a high bacteriological load. Fecal pollution is instituted by means of septic tanks, which contribute to input fecal germs directly in the aquifer and via surface pollution leaching. In addition, agricultural practices by using manure as natural fertilizer participate in the propagation of bacteriological contaminants. Domestic waste released into abandoned wells also participates in aquifer contamination.

The groundwater pollution risk map based on GCI

The GCI values range from 15 to 32 during the dry season. This index is classified into three categories, which include $\text{GCI} < 20$ (low degree of groundwater contamination), $20 < \text{GCI} < 25$ (moderate to high degree of groundwater

contamination), and $\text{GCI} > 25$ (high degree of contamination index). The groundwater pollution risk map (Fig. 9) shows that the high index values belong to the south and northeast regions, while the low index values are located in the western part of the island. The contaminated parts of the aquifer are affected by several sources of pollution and overexploited. The spatial distribution maps of GCI calculated for 54 wells confirm the contamination of the coastal areas, especially the northern and western parts of the island that are considered as areas of low topography and piezometry. The decrease of the piezometric level in the aquifer generates the inversion of the hydraulic gradient. This fact promotes the transfer of seawater and contaminated waters to the aquifer. The overexploitation of the Mio-Pliocene–Quaternary Jerba aquifer has resulted in a number of drawdown cones, a lower aquifer, and depressions that allow seawater to enter the aquifer (Souid et al. 2018). Souid et al. (2018, 2020) used the traditional geochemical investigation and a simple assessment of the contamination of the Jerba island, but the comparison the GCI elaborated in this study and the other methods (Kharroubi et al. 2012; Telahigue et al. 2018) showed that it is robust and gives the best classification of groundwater quality which is very faithful to the reality of the Island. It includes several parameters that represent the pressures exerted on the aquifer by different components (seawater intrusion, nitrate pollution, and fecal contamination). The calculated GCI values will identify the extent of contamination by combining the different sources of pollution existing on the island. In addition, the usefulness of this index is to assess the groundwater contamination degree and the identification of the major contamination mechanism, by area, depending on the weights assigned to each parameter.

Jerba shallow aquifer is a coastal aquifer under an arid climate, which is influenced by several contamination processes. However, punctual sources of pollution like septic tanks and abandoned wells used as uncontrolled garbage

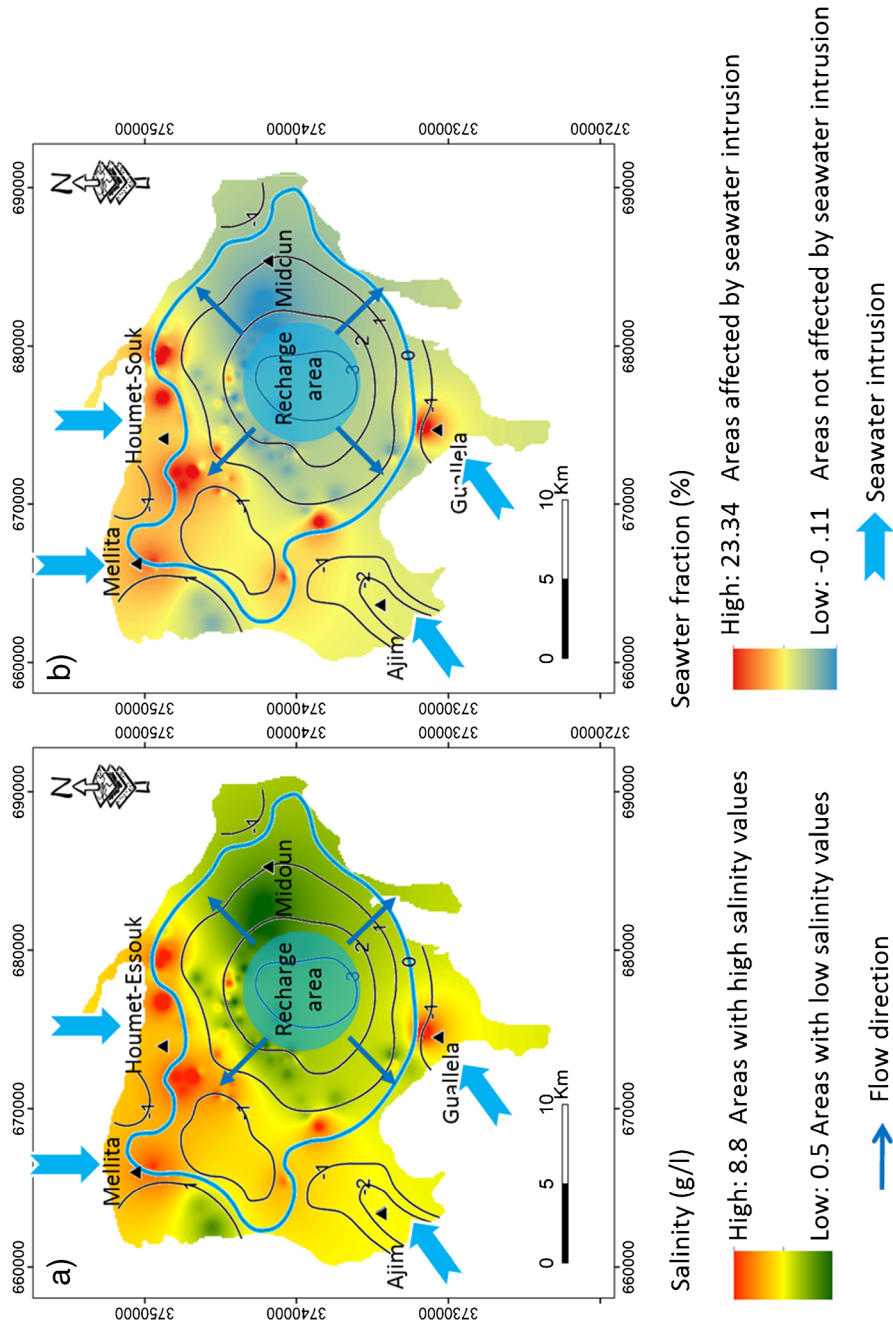


Fig. 7 a The spatial distribution of groundwater salinity correlated with the piezometric level of the aquifer; **b** the spatial distribution of measured seawater fraction

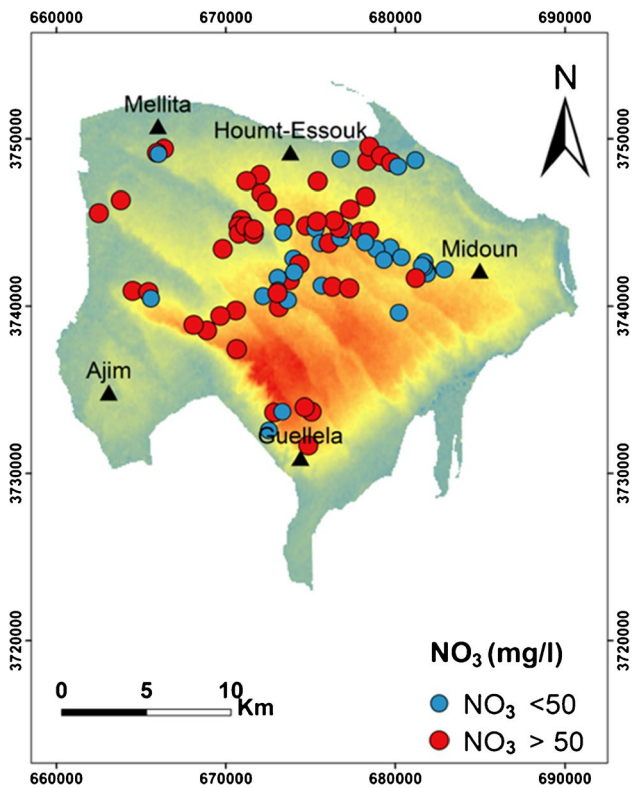


Fig. 8 Spatial distribution of NO_3^- concentration

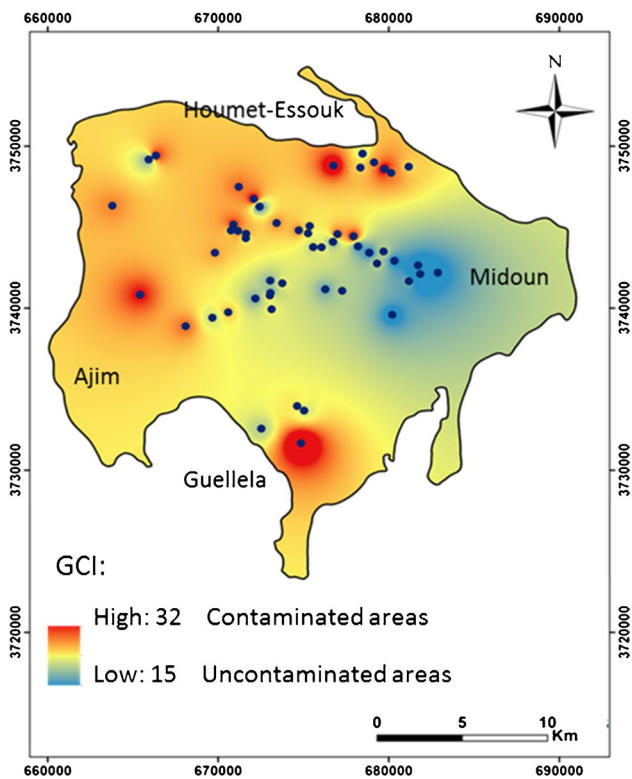


Fig. 9 Spatial distribution pattern of calculated GCI

dumps are considered as direct sources of groundwater pollution. Previous studies carried out by Souid et al. (2017) have shown severe fecal pollution of the aquifer due to the septic tanks. Agricultural practices also led to an increase in nitrate contents and fecal bacteria by the infiltration of irrigation water loaded with fertilizers and germs. The exploited groundwater quantities of unconfined aquifer on Jerba Island reached $3.65 \text{ Mm}^3/\text{year}$ with available resources not exceeding $3.47 \text{ Mm}^3/\text{year}$. This deficit balance between available resources and exploitation with a low rate of groundwater recharge, due to the aridity of the climate, aggravates the situation and promotes seawater intrusion processes.

Conclusion

This study presents an approach for the hydrogeological pollution assessment of arid coastal shallow aquifers. Results of the groundwater contamination index (GCI) in this research demonstrated that groundwater pollution at several sites of the island is very intense. The GCI was calculated by admitting class intervals for lithium and nitrate contents, calculated marine intrusion fraction, and fecal tracers. Assessment of results based on the spatial distribution of pollution degree illustrates that the proposed index reveals that 75.91% of the aquifer comes under a significant pollution zone (the coastal regions of the island). The groundwater pollution risk map shows the areas that are most affected by pollution and have high levels of nitrate, lithium, fecal germs, and a high marine intrusion rate. Areas characterized by high GCI are subject to the combined effect of anthropogenic activities and seawater intrusion. The overexploitation of the aquifer leads to a groundwater balance deficit between exploitation and available resources. These results confirm the impact of two major processes involved in aquifer pollution: seawater intrusion, a process that affects coastal areas and is activated by overpumping, and the anthropogenic impact favored by septic tanks and wells used as dumping grounds.

Declarations

Conflict of interest The authors declare no competing interests.

References

Adimalla N, Qian H, Nadan MJ (2020) Groundwater chemistry integrating the pollution index of groundwater and evaluation of potential human health risk: a case study from hard rock terrain of south India. *Ecotoxicol Environ Saf* 206:111217. <https://doi.org/10.1016/j.ecoenv.2020.111217>

Alcala FJ, Custodio F (2008) Using the Cl/Br ratio as a tracer to identify the origin of salinity in aquifers in Spain and Portugal. *J Hydrol* 359:189–207

- Barilari A, Quiroz London M, Paris M, Lima ML, Massone M (2020) Groundwater contamination from point sources. A hazard index to protect water supply wells in intermediate cities. *Groundw Sustain Dev J* 10:100363
- Besbes M, Chahed J, Hamdane A (2014) Sécurité Hydrique de la Tunisie Gérer l'eau en conditions de penuries, L'HARMATTAN, 2014 5–7, rue de l'École-Polytechnique ; 75005 Paris.
- Bouaziz S, Jedoui Y, Barrier E, Angelier J (2003) Néotectonique affectant les dépôts marins tyrrhéniens du littoral sud-est tunisien: implication pour les variations du niveau marin. *C r Geosci* 335:247–254
- Boudibi S, Sakaa B, Benguega Z (2021) Spatial variability and risk assessment of groundwater pollution in El-Outaya region, Algeria. *Journal of African Earth Sciences* 176:104135
- Boudibi S, Sakaa B, Benguega Z, Fadlaoui H, Othman T, Bouzidi N (2021) Spatial prediction and modeling of soil salinity using simple cokriging, artificial neural networks, and support vector machines in El Outaya plain, Biskra, southeastern Algeria. *Acta Geochim* 40:390–408
- Burgess TM, Webster R (1980) Optimal interpolation and isarithmic mapping of soil properties The semi-variogram and punctual kriging. *J Soil Sci* 31:315–331
- Busico G, Cuoco E, Kazakis N, Colombani N, Mastrocicco M, Tedesco D, Voudouris K (2018) Multivariate statistical analysis to characterize/discriminate between anthropogenic and geogenic trace elements occurrence in the Campania Plain, Southern Italy. *Environ Pollut* 234:260–269
- Carol ES, Alvarez MDP, Tanjal C, Bouza PJ (2021) Factors controlling groundwater salinization processes in coastal aquifers in semiarid environments of north Patagonia, Argentina. *J S Am Earth Sci* 110:103356
- Cartwright I, Weaver TR, Fifield Keith L (2006) Cl/Br ratios and environmental isotopes as indicators of recharge variability and groundwater flow: an example from the southeast Murray Basin, Australia. *Chem Geol* 231:35–56
- Elliott AC, Woodward WA (2007) Statistical analysis quick reference guide book with SPSS examples, 1st edn. Sage Publications, London
- Elloumi (2016) La gouvernance des eaux souterraines en Tunisie, International water management institute project report groundwater governance in the Arab World Report no.6, 115
- Ghasemi A, Saleh Zahedi S (2012) Normality tests for statistical analysis: a guide for non-statisticians. *Int J Endocrinol Metab* 10(2):486–489. <https://doi.org/10.5812/ijem.3505>
- Hamdi M, Zagarni MF, Tarhouni J (2017) Hydrogeochemical and isotopic investigation and water quality assessment of groundwater in the Sisseb El Alem Nadhour Saouaf aquifer (SANS), northeastern Tunisia. *J Afr Earth Sc* 141:148–163
- Han Tran N, Yew-Hoong Gin K, Hao Ngo H (2015) Fecal pollution source tracking toolbox for identification, evaluation and characterization of fecal contamination in receiving urban surface waters and groundwater. *Sci Total Environ* 538:38–57
- Hatvani IG, Szatmari G, Kern Z, Erdélyi D, Vreca P, Kanduc T, Czuppon G, Lojen S, Kohan B (2021) Geostatistical evaluation of the design of the precipitation stable isotope monitoring network for Slovenia and Hungary. *Environ Int J* 146:106263
- He S, Li P, Su F, Wang D, Ren X (2022) Identification and apportionment of shallow groundwater nitrate pollution in Weining Plain, northwest China, using hydrochemical indices, nitrate stable isotopes, and the new Bayesian stable isotope mixing model (Mix-SIAR). *Environ Pollut* 298:118852
- He S, Wu J, Wanga D, He X (2022) Predictive modeling of groundwater nitrate pollution and evaluating its main impact factors using random forest. *Chemosphere* 290:133388
- Herojeet R, Naik PK, Rishi MS (2020) A new indexing approach for evaluating heavy metal contamination in groundwater. *Chemosphere* 245:125598. <https://doi.org/10.1016/j.chemosphere.2019.125598>
- Innocent C, Millot R, Kloppmann W (2021) A multi-isotope baseline (O, H, C, S, Sr, B, Li, U) to assess leakage processes in the deep aquifers of the Paris basin (France). *Appl Geochem* 131:105011
- Jedoui Y (2000) Sédimentologie et géochimie des Dépôt littoraux quaternaires: reconstitution des variations des climats et du niveau marin dans le sud est tunisien. PhD. Thesis in geologic sciences, University of Tunis, Tunisia.
- Johnston K, Ver Hoef JM, Krivoruchko K, Lucas N (2001) Using ArcGIS geostatistical analyst. Esri, Redlands, p. 380.
- Kharroubi A, Tlahigue F, Agoubi B, Azri C, Bouri S (2012) Hydrochemical and statistical studies of the groundwater salinization in Mediterranean arid zones: case of the Jerba coastal aquifer in southeast Tunisia. *Environ Earth Sci* 67:2089–2100
- Kou X, Ding J, Li Y, Li Q, Mao L, Xu C, Zheng Q, Zhuang S (2021) Tracing nitrate sources in the groundwater of an intensive agricultural region. *J Agric Water Manag* 250:106826
- Koné M, Bonou L, Bouvet Y, Joly P, Kouliadiaty J (2009) Etude de la pollution des eaux par les intrants agricoles: cas de cinq zones d'agriculture intensive du Burkina Faso. *Sud Sciences et Technologies* 17:6–15
- Kumar PJS (2014) Evolution of groundwater chemistry in and around Vaniyambadi industrial area: differentiating the natural and anthropogenic sources of contamination. *Chem Erde Geochem* 74:641–651. <https://doi.org/10.1016/j.chemer.2014.02.002>
- Li P, He X, Guo W (2019) Spatial groundwater quality and potential health risks due to nitrate ingestion through drinking water: a case study in Yan'an City on the Loess Plateau of northwest China, Human and Ecological Risk Assessment: An International Journal 25, Issue 1–2: Special issue: Sustainable Living with Risks, <https://doi.org/10.1080/10807039.2018.1553612>
- Ma J, Ding Z, Wei G, Zhao H, Huang T (2009) Sources of water pollution and evolution of water quality in the Wuwei basin of Shiyang river, Northwest China. *J Environ Manag* 90(2):1168–1177
- Mahlangu S, Lorentz S, Diamond R, Dippenaar M (2020) Surface water-groundwater interaction using tritium and stable water isotopes: a case study of Middelburg, South Africa. *J Afr Earth Sc* 171:103886
- Mathuthua M, Uushona V, Indongoa V (2020) Radiological safety of groundwater around a Uranium mine in Namibia. *Phys Chem Earth* 122(1):102915
- McArthur JM, Sikdar PK, Hoque MA, Ghosal U (2012) Waste-water impacts on groundwater: Cl/Br ratios and implications for arsenic pollution of groundwater in the Bengal Basin and Red River Basin, Vietnam. *Sci Total Environ* 437:390–402
- Milena-Pérez A, Pinero-García F, Benavente J, Exposito-Suarez VM, Vacas-Arquero P, Ferro-García MA (2020) Uranium content and uranium isotopic disequilibria as a tool to identify hydrogeochemical processes. *J Environ Radioact* 227:106503
- Nagarajan R, Rajmohan N, Mahendran U, Senthilkumar S (2010) Evaluation of groundwater quality and its suitability for drinking and agricultural use in Thanjavur city. Tamil Nadu, India, *Environ Monit Assess* 171:289–308. <https://doi.org/10.1007/s10661-009-1279-9>
- Nigro A, Sappa G, Barbieri M (2017) Application of boron and tritium isotopes for tracing landfill contamination in groundwater. *J Geochem Explor* 172:101–108
- Nisi B, Vaselli O, Taussi M, Doveri M, Menichini M, Cabassi J, Raco B, Botteghi S, Mussi M, Masetti G (2022) Hydrogeochemical surveys of shallow coastal aquifers: A conceptual model to set-up a monitoring network and increase the resilience of a strategic groundwater system to climate change and anthropogenic pressure. *Appl Geochem* 142: 105350
- Nsabimana A, Li P, He S, He X, Khorshed Alam SM (2021) Misbah F (2021) Health risk of the shallow groundwater and its suitability

- for drinking purpose in Tongchuan, China. *Water* 13(22):3256. <https://doi.org/10.3390/w13223256>
- Oztuna D, Elhan AH, Tuccar E (2006) Investigation of four different normality tests in terms of type 1 error rate and power under different distributions. *Turk J Med Sci* 36(3):171–176
- Patel M, Gami B, Patel A, Patel P, Patel B (2020) Climatic and anthropogenic impact on groundwater quality of agriculture dominated areas of southern and central Gujarat, India. *Groundw Sustain Dev* 10:100306. <https://doi.org/10.1016/j.gsd.2019.100306>
- Peat J, Barton B (2005) *Medical statistics: a guide to data analysis and critical appraisal*. Blackwell Publishing.
- Rao NS, Shoudhary M (2019) Hydrogeochemical processes regulating the spatial distribution of groundwater contamination, using pollution index of groundwater (PIG) and hierarchical cluster analysis (HCA): a case study. *Groundw Sustain Dev J* 9:100238
- Rufino F, Busico G, Cuoco E, Darrah TH, Tedesco D (2019) Evaluating the suitability of urban groundwater resources for drinking water and irrigation purposes: an integrated approach in the Agro-Aversano area of Southern Italy. *Environ Monit Assess* 191:768. <https://doi.org/10.1007/s10661-019-7978-y>
- Serra J, Cameira MDR, Cordovil CMDS, Hutchings NJ (2021) Development of a groundwater contamination index based on the agricultural hazard and aquifer vulnerability: application to Portugal. *Sci Total Environ J* 722:145032
- Silva MI, Gonçalves ML, Lopes WA, Lima MTV, Costa CTF, Paris M, Firmino PRA, De Paula Filho FJ (2021) Assessment of groundwater quality in a Brazilian semiarid basin using an integration of GIS, water quality index and multivariate statistical techniques. *J Hydrol* 598:126346
- Solgi E, Jalili M (2021) Zoning and human health risk assessment of arsenic and nitrate contamination in groundwater of agricultural areas of the twenty two village with geostatistics (Case study: Chahardoli Plain of Qorveh, Kurdistan Province, Iran). *Agric Water Manag* 255:107023. <https://doi.org/10.1016/j.agwat.2021.107023>
- Somarathne N, Zulfic H, Ashman G, Vial H, Swaffer B, Frizenschaf J (2013) Groundwater risk assessment model (GRAM): groundwater risk assessment model for wellfield protection. *Water* 5:1419–1439. <https://doi.org/10.3390/w5031419>
- Souid F, Agoubi B, Kharroubi A (2017) Assessing the groundwater pollution problem by nitrate and faecal bacteria: case of Djerba unconfined aquifer (Southeast Tunisia). *Water and Land Security in Drylands*. https://doi.org/10.1007/978-3-319-54021-4_9
- Souid F, Agoubi B, Telahigue F, Chahlaoui A, Kharroubi A (2018) Groundwater salinization and seawater intrusion tracing based on lithium concentration in the shallow aquifer of Jerba Island, southeastern Tunisia. *J Afr Earth Sc* 138:233–246
- Souid F, Agoubi B, Telahigue F, Kharroubi A (2020) Isotopic behavior and self-organizing maps for identifying groundwater salinization processes in Jerba Island, Tunisia. *Environ Earth Sci J* 79:175
- Teissier J (1967) Hydrogeological study of Jerba unconfined aquifer. Water Resources Direction. Ministry of Agriculture, Tunisia.
- Telahigue F, Agoubi B, Souid F, Kharroubi A (2018) Groundwater chemistry and radon-222 distribution in Jerba Island Tunisia. *J Environ Radioact* 182:74–84
- Visentini AF, Linde N, Borgne TL, Dentz M (2020) Inferring geostatistical properties of hydraulic conductivity fields from saline tracer tests and equivalent electrical conductivity time-series. *Adv Water Resour J* 146:1037583
- Wagh VM, Panaskar DB, Mukate SV, Gaikwad SK, Muley AA, Varade AM (2018) Health risk assessment of heavy metal contamination in groundwater of Kadava River Basin, Nashik, India. *Model Earth Syst Environ* 4(3):969–980
- Yahyaoui H (2012) Nappe phréatique de l'île de Jerba: aspects hydrogéologiques et mobilisation des ressources. Ministère de l'Agriculture: rapport interne du Commissariat Régionale De l'Agriculture de Medenine, Tunisie.
- Zaporozec A (2004) Groundwater contamination inventory: a methodological guide. Issue 2 of IHP-VI series on groundwater. Volume 2 of International Hydrological Programme. UNESCO, Paris.
- Zare-Mehrjardi M, Taghizadeh-Mehrjardi R, Akbarzadeh A (2010) Evaluation of geostatistical techniques for mapping spatial distribution of soil pH, salinity and plant cover affected by environmental factors in southern Iran. *Notulae Scientia Biologicae* 2(4):92–103. <https://doi.org/10.15835/nsb244997>
- Zhang Y, Dai Y, Wang Y, Huang X, Xiao Y, Pei Q (2021) Hydrochemistry, quality and potential health risk appraisal of nitrate enriched groundwater in the Nanchong area, southwestern China. *Sci Total Environ J* 784:147186

Springer Nature or its licensor holds exclusive rights to this article under a publishing agreement with the author(s) or other rightsholder(s); author self-archiving of the accepted manuscript version of this article is solely governed by the terms of such publishing agreement and applicable law.